

REGULAR ARTICLE

Bayesian sparse modeling for interpretable prediction of hydroxide ion conductivity in anion-conductive polymer membranes

Ryo Murakami^a, Kenji Miyatake^{b,c}, Ahmed Mohamed Ahmed Mahmoud^{b,d}, Hideki Yoshikawa^a, Kenji Nagata^e

^aResearch Network and Facility Services Division, National Institute for Materials Science, Tsukuba 305-0044, Ibaraki, Japan;

^bClean Energy Research Center, University of Yamanashi, Kofu 400-8510, Yamanashi, Japan;

^cDepartment of Applied Chemistry, Waseda University, Tokyo 169-8555, Japan;

^dOffice of Institutional Advancement and Communications, Kyoto University, Kyoto 6068501, Japan;

^eCenter for Basic Research on Materials, National Institute for Materials Science, Tsukuba 305-0044, Ibaraki, Japan

ARTICLE HISTORY

Compiled May 27, 2025

ABSTRACT

Anion-conductive polymer membranes have attracted considerable attention as solid electrolytes for alkaline fuel cells and electrolysis cells. Their hydroxide ion conductivity varies depending on factors such as the type and distribution of quaternary ammonium groups, as well as the structure and connectivity of hydrophilic and hydrophobic domains. In particular, the size and connectivity of hydrophilic domains significantly influence the mobility of hydroxide ions; however, this relationship has remained largely qualitative. In this study, we calculated the number of key constituent elements in the hydrophilic and hydrophobic units based on the copolymer composition, and investigated their relationship with hydroxide ion conductivity by using Bayesian sparse modeling. As a result, we successfully identified composition-derived features that are critical for accurately predicting hydroxide ion conductivity.

KEYWORDS

anion-conductive polymer membranes; Materials informatics; Data-driven science; Sparse modeling; Bayesian inference

1. Introduction

Anion-conductive polymer membranes are promising candidates for use as solid electrolytes in alkaline energy devices, such as fuel cells and water electrolysis cells. In particular, anion exchange membrane water electrolysis systems, which can produce green hydrogen efficiently by utilizing renewable energy sources, are being actively investigated worldwide as a core technology for realizing a carbon-neutral hydrogen society. For such applications, desirable properties of anion-conductive polymers include anion conductivity comparable to that of alkaline aqueous electrolytes, the ability to form thin membranes (thickness $< 50\mu\text{m}$) with sufficient mechanical strength, gas

CONTACT Ryo Murakami. Email: MURAKAMI.Ryo@nims.go.jp

CONTACT Kenji Miyatake. Email: miyatake@yamanashi.ac.jp

barrier properties against hydrogen and oxygen, and water permeability and alkaline stability under low-humidity conditions. Among these, hydroxide ion conductivity is the most critical property, as it directly determines the voltage efficiency of anion exchange membrane water electrolysis systems.

Anion-conductive polymers are generally composed of hydrophobic polymer backbones functionalized with cationic groups. While a variety of backbones—including aliphatic and aromatic types—are available, it is known that structures without heterobonds such as ether linkages in the main chain are preferable from the viewpoint of alkaline stability [1]. Onium salts are commonly employed as cationic functional groups due to their synthetic accessibility, ease of incorporation into polymers, and adequate hydroxide ion dissociation; among them, quaternary ammonium groups are known to provide high anion conductivity. In general, the ion exchange capacity (IEC) of quaternary ammonium groups has a major impact on conductivity—higher IEC values typically correspond to higher hydroxide ion conductivity in thin membranes. However, even at similar IEC values, the conductivity can vary depending on the polymer backbone, the type of ammonium group, and their combination, as well as the connectivity of hydrophilic and hydrophobic domains. This is because quaternary ammonium groups and water molecules can aggregate to form hydrophilic domains, and the size, connectivity, and tortuosity of these domains significantly affect hydroxide ion mobility.

Hydrophilic domain structures can be analyzed by various experimental techniques. For instance, small-angle X-ray scattering (SAXS) provides information on the shape and periodicity of hydrophilic domains, while transmission electron microscopy (TEM) allows direct observation of domain size and connectivity [2]. Atomic force microscopy (AFM) can distinguish hydrophilic and hydrophobic domains on the membrane surface based on phase contrast, and electrochemical AFM can visualize ion-conductive pathways as current responses during oxidation or reduction reactions. Although these techniques provide valuable insights into the phase-separated morphology of the membrane, most discussions to date have remained qualitative, and a quantitative understanding has not been established. Moreover, cases where membranes exhibit similar morphologies and IECs but differ in hydroxide ion conductivity remain unresolved.

In this study, we aimed to quantitatively understand the variation in conductivity among a series of anion-conductive polymer membranes previously developed by our group [3–6]. We calculated the number of key constituent elements in the hydrophilic and hydrophobic units, taking into account the copolymer composition, and examined their potential as predictive features for hydroxide ion conductivity. Our goal was to construct an interpretable and low-dimensional predictive model using a linear analytical framework. Since the set of important features is not known a priori, we generated multiple candidate features and performed both conductivity prediction and feature selection simultaneously, as illustrated in Figure 1.

2. Dataset outline

In this study, the target variable was defined as the hydroxide ion conductivity of anion-conductive polymer membranes measured in water at 30°C, along with the structural characteristics of their hydrophilic and hydrophobic domains. It is well known that anion conductivity correlates with several physical parameters of the polymer membranes, including ion exchange capacity (IEC), water uptake, and the size and connectivity of hydrophilic clusters. Generally, a higher IEC leads to an increased

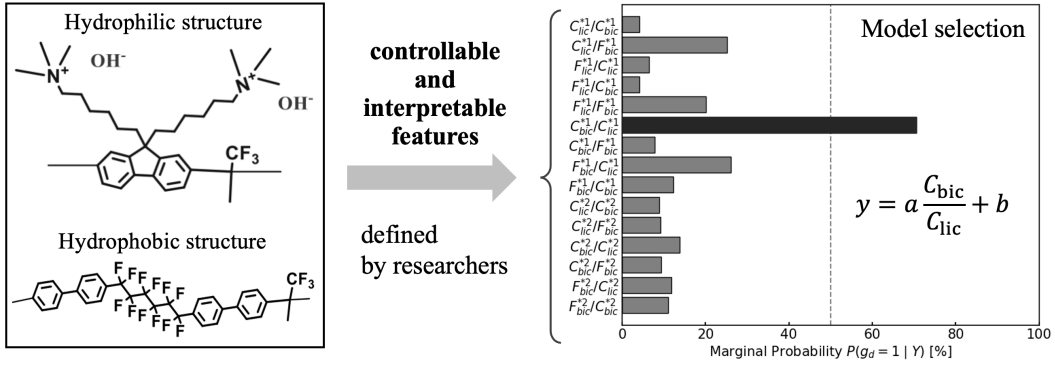


Figure 1. Overview diagram of this study. We design controllable and interpretable candidate features from the chemical structures shown on the left side. Then, as shown on the right side, we explore equations that describe material properties (conductivity) by using model selection based on the marginal log-likelihood in Bayesian estimation framework.

carrier concentration and, consequently, higher conductivity. However, excessive IEC can result in increased water uptake—particularly in terms of the number of water molecules adsorbed per ionic group—thereby reducing the effective carrier density and leading to lower conductivity.

The hydrophilic clusters in anion-conductive polymer membranes can be visualized from transmission electron microscopy (TEM) images of samples in which the ammonium groups were selectively stained by ion exchange with PtCl_4^{2-} ions. It is expected that larger hydrophilic clusters provide more continuous conduction pathways, leading to higher ion mobility and thus higher conductivity. Figure 2 shows scatter plots of hydroxide ion conductivity versus the average diameter of hydrophilic and hydrophobic clusters estimated from TEM images. However, no clear correlation was observed in either case, indicating that cluster size alone is insufficient to describe conductivity, especially when the polymer structures differ.

We hypothesize that the number of carbon (C) and fluorine (F) atoms in the hydrophilic and hydrophobic units influences the spatial occupation, domain size, and connectivity within the polymer structure, thereby functioning as key structural descriptors governing hydroxide ion conductivity. Therefore, in this study, we calculated the number of C and F atoms based on the copolymer composition for each segment and investigated whether these values could serve as predictive features for conductivity. The dataset used in this study consisted of 18 polymer samples [3–6], and the number of explanatory variables (features) was 15. We refer you to the subsection 3.2 for details on features.

3. Method

3.1. Analysis outline

Our purpose is to identify explanatory features that describe the hydroxide ion conductivity of anion-conductive polymer membranes. Figure 3 shows an overview of the analytical workflow. As illustrated in Figure 3, we focus on linear models from the perspectives of interpretability and robustness. We hypothesize that, in local regions of the design space with finite data, meaningful correlations can be captured even

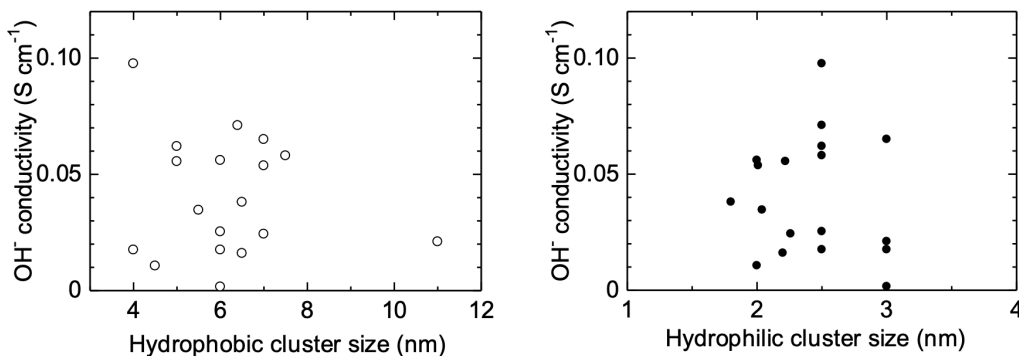


Figure 2. Scatter plot of conductivity against the average diameter of (left) hydrophobic cluster size and (right) hydrophilic cluster size obtained from TEM images [3–6].

with a linear model, provided the constructed features contain sufficient information. Accordingly, we begin by using interpretable and controllable compositional features to predict conductivity via linear regression. The details of the regression model are described in the following subsection.

By constructing a predictive model based on compositional features that can be experimentally controlled, we aim to support the design of future experiments. However, in the materials domain, datasets often contain a limited number of samples, and including too many features can lead to overfitting and poor generalization performance. At the same time, it is not obvious which features are most strongly correlated with conductivity.

To address this, as shown in Figure 3, we generate multiple candidate features and perform not only conductivity prediction but also simultaneous feature selection. For this purpose, we employ a Bayesian linear regression model with automatic feature selection. The methodology for selecting relevant features is described in the next section. By identifying a minimal set of features that can describe conductivity, we can suppress overfitting and obtain a more robust model. Furthermore, it is well known that lower-dimensional feature spaces are advantageous when designing follow-up experiments.

3.2. Description of features

In this study, we calculated the number of carbon (C) and fluorine (F) atoms in the hydrophilic and hydrophobic units of each polymer, taking into account the copolymer composition, and investigated whether these values could serve as effective features for predicting hydroxide ion conductivity. This approach is based on the hypothesis that the number of C and F atoms is related to the spatial occupancy of the polymer structure, as well as to the size and connectivity of hydrophilic and hydrophobic domains—factors that are believed to govern hydroxide ion conductivity.

In particular, the number of carbon atoms is expected to influence the rigidity or flexibility of the polymer backbone and side chains, the intermolecular distances, and the ability to form well-organized domain structures. These, in turn, affect the continuity and hydration of the hydrophilic network. On the other hand, the number of fluorine atoms may influence the hydrophobicity and electron density of the polymer, potentially affecting the formation and stability of ion-conducting pathways.

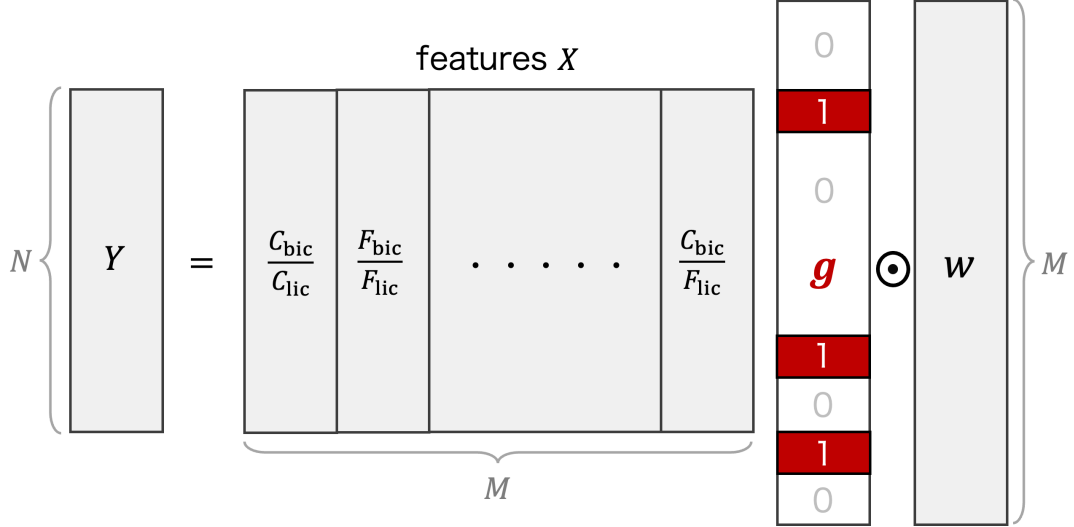


Figure 3. An overview diagram of linear regression with indicators to select a model (feature combination). Y and X are object and explanatory variable (candidate features), respectively. g and w are indicator (0 or 1) vector and weight coefficient parameters. N and M are the number of data samples and candidate features, respectively.

We examined two definitions for distinguishing hydrophilic and hydrophobic units:

- *1) Direct assignment based on the chemical structure of the repeating units in the polymer backbone;
- *2) A more selective definition in which only side chain structures containing ammonium groups (composed exclusively of sp^3 -hybridized carbon atoms and presumed to readily form hydrophilic domains) are classified as hydrophilic, and all other structures are classified as hydrophobic.

These two definitions are hereafter referred to as *1 and *2, respectively.

3.3. Bayesian linear regression with feature selection

A Bayesian linear regression model with feature selection [7–9] can be formulated using input features $x_n \in \mathbb{R}^M$ and output material properties $y_n \in \mathbb{R}$ as follows:

$$y_n = \mathbf{x}_n(\mathbf{g} \odot \mathbf{w})^\top + \varepsilon_n, \quad \varepsilon_n \sim \mathcal{N}(\mu = 0, \sigma^2 = \lambda^{-1}). \quad (1)$$

where $\mathbf{g} \in \{0, 1\}^M$ is a binary indicator vector used to select relevant features, $\mathbf{w} \in \mathbb{R}^M$ is the weight coefficient vector, and $\lambda \in \mathbb{R}$ is the precision parameter. The operator \odot denotes the Hadamard (element-wise) product. When $g_m = 1$, the m -th feature $x_{:,m}$ is considered necessary for predicting the material property; conversely, $g_m = 0$ indicates that the feature is not required. The noise term ε_n is assumed to follow a normal distribution, $\mathcal{N}(\mu = 0, \sigma^2 = \lambda^{-1})$. Accordingly, the likelihood of the dataset $\mathcal{D} = \{(\mathbf{x}_n, y_n)\}_{n=1}^N$ consisting of N samples can be expressed as:

$$P(\mathcal{D} | \mathbf{g}, \mathbf{w}, \lambda) = \prod_{n=1}^N P(y_n | \mathbf{g}, \mathbf{w}, \lambda, \mathbf{x}_n) = \prod_{n=1}^N \mathcal{N}(\mu = \mathbf{x}_n(\mathbf{g} \odot \mathbf{w})^\top, \sigma^2 = \lambda^{-1}). \quad (2)$$

Accordingly, the posterior distribution of the indicator vector \mathbf{g} , denoted as $P(\mathbf{g} | Y)$, can be expressed as follows:

$$P(\mathbf{g} | \mathcal{D}) \propto P(\mathcal{D} | \mathbf{g})P(\mathbf{g}) = \iint P(\mathcal{D} | \mathbf{g}, \mathbf{w}, \lambda)P(\mathbf{g})P(\mathbf{w})P(\lambda)d\mathbf{w}d\lambda \quad (3)$$

Here, $P(\mathbf{g})$, $P(\mathbf{w})$, and $P(\lambda)$ represent the prior distributions for each parameter. These priors are defined as follows:

$$P(\mathbf{g}) = \prod_{m=1}^M \mathcal{B}(g_m | p_B), \quad (4)$$

$$P(\mathbf{w}) = \prod_{m=1}^M \mathcal{N}(w_m | \mu_N, \sigma_N^2), \quad (5)$$

$$P(\lambda) = \mathcal{G}(\lambda | k_G, \theta_G), \quad (6)$$

where $\mathcal{B}(g | p_B)$, $\mathcal{N}(w | \mu_N, \sigma_N^2)$, and $\mathcal{G}(\lambda | k_G, \theta_G)$ represent the Bernoulli, Normal, and Gamma distributions, respectively. In equation (3), marginalization over the weight parameter \mathbf{w} was performed analytically, while marginalization over the precision parameter λ was carried out using numerical integration.

In this study, we approximated an exhaustive search over all possible indicator states using the exchange Monte Carlo method [10–12], based on the probability defined in equation (3). The marginal posterior probability that the m -th feature is selected can be expressed as follows:

$$P(g_m = 1 | \mathcal{D}) = \sum_{\{\mathbf{g} | g_m=1\}} P(\mathbf{g} | \mathcal{D}) \quad (7)$$

4. Experimental configuration

In this study, we used the exchange Monte Carlo method to estimate the post-distribution of indicators. The burn-in period was set to 10000 iterations, and 10000 samples were drawn for inference. In the exchange monte carlo method, we set the reverse temperature β as follows: $\beta = \{\rho^{t-T} | t = \{1, 2, \dots, T\}\}$ where the number of temperature T and the proportion ρ were set to $T = 46$ and $\rho = 1.1$, respectively.

We set the hyperparameters of the prior distribution as follows: $p_B = 0.5$, $\mu_N = 0$, $\sigma_N^2 = 1.0$, $k_G = 1.5$, $\theta_G = 10$. The computations were performed on a MacBook Air equipped with an Apple M2 chip and 24 GB of RAM.

5. Results and discussion

The results of feature selection are shown in Figure 4. In this figure, the y-axis represents the labels of candidate features, and the x-axis corresponds to the marginal posterior probability of the indicator variable for each feature, denoted as $P(g_m = 1 | \mathcal{D})$. Since the prior distribution for the indicator variable was set as a Bernoulli distribution $\mathcal{B}(p_B = 0.5)$, a posterior probability exceeding 50% indicates that the corresponding feature is considered important for the prediction task.

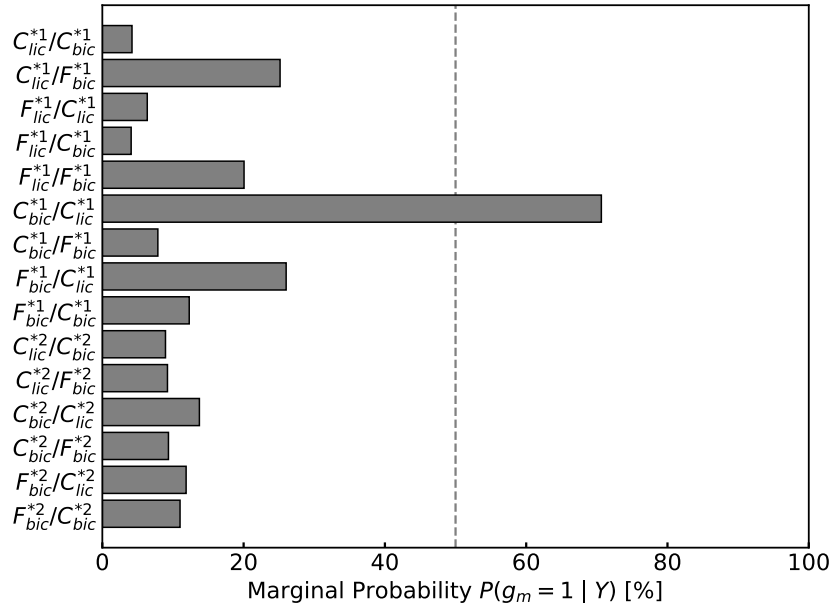


Figure 4. Result of feature selection based on the marginal log-likelihood. Candidate features was defined from composition information. The wavy line indicates the prior probability of 50%. Object variable is conductivity.

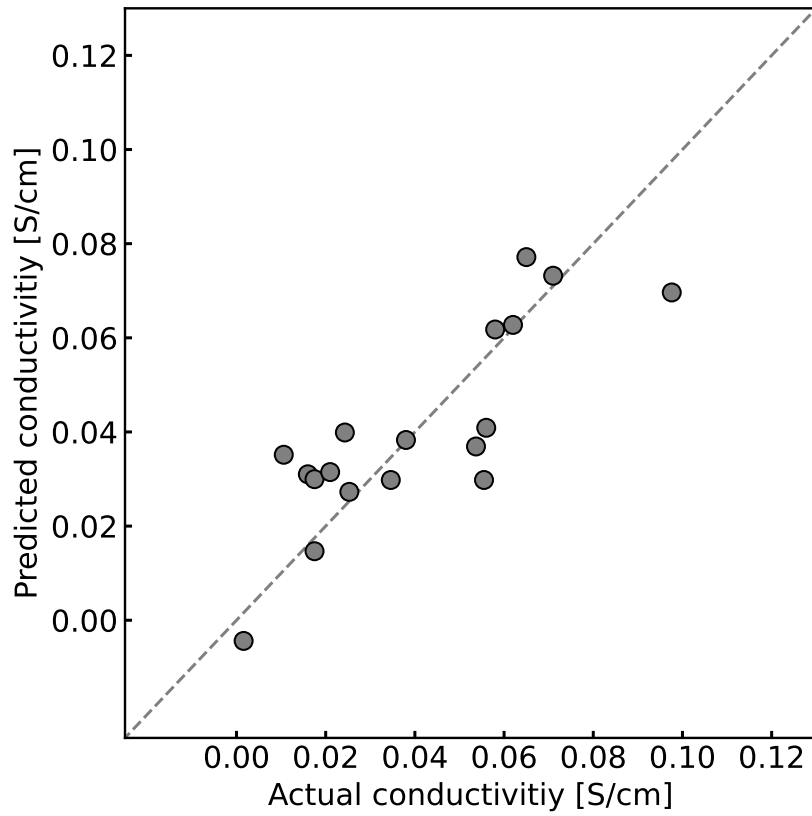


Figure 5. Conductivity prediction result based on selected model: $\hat{y} = aC_{bic}^{(*1)}/C_{lic}^{(*1)} + b$ where $a \approx -0.035$ and $b \approx 0.09$.

From Figure 4, it is evident that the ratio of carbon atoms in the hydrophobic and hydrophilic units, $C_{bic}^{(*1)}/C_{lic}^{(*1)}$, is identified as the most significant feature for predicting hydroxide ion conductivity in this dataset. The marginal probabilities for all other features remain below 50%, suggesting that $C_{bic}^{(*1)}/C_{lic}^{(*1)}$ alone captures the underlying trend of conductivity in this dataset. This result is non-trivial and highlights the unique importance of this compositional ratio.

Accordingly, the trend of hydroxide ion conductivity in this dataset can be expressed as follows:

$$\hat{y} = a \frac{C_{bic}^{(*1)}}{C_{lic}^{(*1)}} + b, \quad (8)$$

where the estimated coefficients were $a \approx -0.035$ and $b \approx 0.09$. This finding—that the ratio of carbon atoms in the hydrophobic and hydrophilic units, $C_{bic}^{(*1)}/C_{lic}^{(*1)}$, exhibits a strong correlation with hydroxide ion conductivity—is novel. Within the present dataset, the carbon content ratio was found to be the most influential factor in determining conductivity, compared to other elemental compositions. This result is also supported by physicochemical reasoning.

It would be probably reasonable that when the hydrophobic units contain a large number of carbon atoms, the hydrophobic domains within the polymer membrane become more dominant. This expansion reduces the connectivity and size of the hydrophilic domains, which can interrupt continuous hydroxide ion transport pathways and consequently lower ionic mobility. In contrast, when the hydrophilic units contain a relatively greater number of carbon atoms, the hydrophilic domains—particularly those containing ammonium groups—tend to become larger, more hydrated, and better connected, thereby enhancing ion transport efficiency. Therefore, the ratio $C_{bic}^{(*1)}/C_{lic}^{(*1)}$ can be interpreted as a descriptor for the formation of effective ion transport pathways, and it exerts a strong influence on hydroxide ion conductivity as a result.

From Figure 4, it was found that, between the following two definitions of hydrophilic and hydrophobic units. The *1 definition yielded more effective features for predicting hydroxide ion conductivity, as indicated by the data-driven analysis. Figure 5 shows the regression results of the predictive model constructed based on the marginal posterior probability. As shown in Figure 5, the model, despite being based on a single feature, is capable of capturing the trend in conductivity. The RMSE (Root Mean Squared Error) was 0.014 [S/cm].

We successfully constructed an interpretable predictive model for this dataset. In materials informatics, where the number of available data points is often limited, predictive models with a small number of features are advantageous because they reduce the risk of overfitting and provide more robust predictions. Therefore, such simplified models can serve as valuable tools for guiding subsequent experimental design.

It should be noted that the dataset used in this study consists of only 18 samples, and the resulting predictive model reflects the trends observed within this specific dataset. Therefore, to evaluate the generalizability and reproducibility of the model, further accumulation of experimental data and validation using external datasets are required.

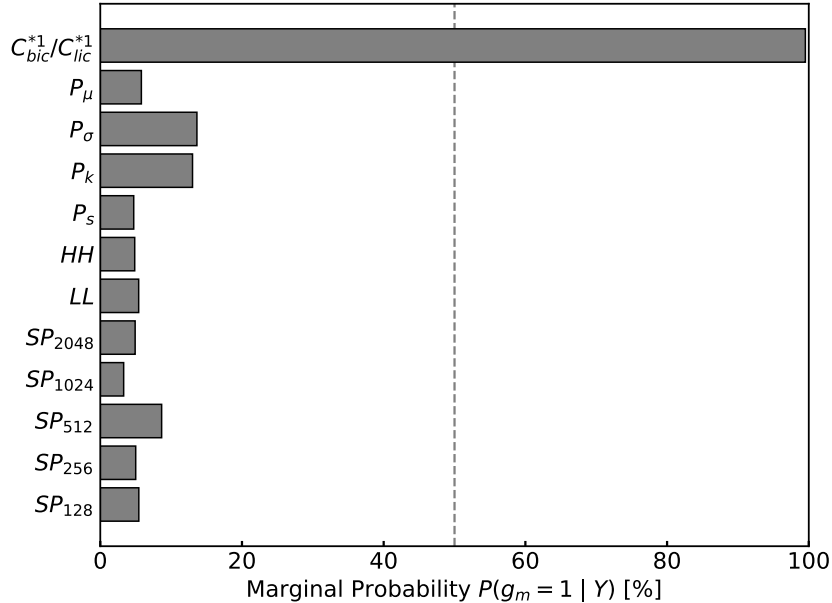


Figure 6. Result of feature selection based on the marginal log-likelihood. Candidate features was $C_{bic}^{(*1)}/C_{lic}^{(*1)}$ and frequency features of TEM images. The wavy line indicates the prior probability of 50%. Object variable is conductivity. We used the TEM image features as follows: brightness statistics $P_\mu, P_\sigma, P_k, P_s$, and frequency-domain features $HH, LL, SP_{2048}, SP_{1024}, SP_{256}, SP_{128}$ obtained via wavelet transformation [13]. The SP_* is an abbreviation for the steerable pyramids, and the subscript indicates the size of the filtered image.

6. Additional Experiments

6.1. Attempt to build a prediction model with added TEM features

In this study, we successfully constructed an interpretable predictive model based on the present dataset. However, as shown in Figure 5, there are several data points around 0.04 [S/cm] where the model exhibits low sensitivity. This observation suggests that while the primary trend in conductivity can be captured by the compositional feature $C_{bic}^{(*1)}/C_{lic}^{(*1)}$, there may be secondary trends that are not fully accounted for. To address this, we attempted to extract complementary information from transmission electron microscopy (TEM) images that could augment the compositional descriptor $C_{bic}^{(*1)}/C_{lic}^{(*1)}$.

TEM images are high-dimensional data, as each pixel represents a feature. Given that the TEM images of the anion-conductive membranes exhibit patterned textures, we extracted two types of features: brightness statistics $P_\mu, P_\sigma, P_k, P_s$, and frequency-domain features $HH, LL, SP_{2048}, SP_{1024}, SP_{256}, SP_{128}$ obtained via wavelet transformation [13]. Each feature is explained in Appendix 8.1.

To extract the frequency features \mathcal{F} , we employed the pyrtools library [14,15], a powerful toolkit for multiscale image analysis. Specifically, Gabor filters with varying scales and orientations were applied, and the spatial average of each filtered image was used as a feature. The number of scales and orientations was set to 5 and 4, respectively. Since the TEM images of the membranes do not exhibit strong orientation preferences, we averaged the results across all orientations. In this analysis, we defined the explanatory variables as $X = C_{bic}^{(*1)}/C_{lic}^{(*1)} \cup \mathcal{F}$, and conducted Bayesian linear

regression with automatic feature selection.

Figure 6 shows the results of feature selection. The y-axis represents feature labels, and the x-axis indicates the marginal posterior probability for each feature, $P(g_m = 1 \mid \mathcal{D})$. As seen in Figure 6, the compositional feature $C_{bic}^{(*1)}/C_{lic}^{(*1)}$ was selected with nearly 100% probability, whereas all frequency-domain features from set \mathcal{F} were selected with probabilities below 50%.

These results suggest that the compositional feature already encapsulates the essential structural information that would otherwise be captured from the TEM images. In other words, the frequency features derived from the images do not provide additional information for predicting hydroxide ion conductivity. This implies that the banded structures observable in the TEM images—reflected in the frequency-domain features—are predominantly determined by the underlying chemical structure. The verification of this suggestion is shown in Appendix 8.2.

7. Conclusion

This study aimed to identify key features that describe hydroxide ion conductivity in anion-conductive polymer membranes. To achieve this, we constructed a predictive model using Bayesian linear regression with automatic feature selection. As a result, we found that the ratio of carbon atoms in the hydrophobic and hydrophilic units, $C_{bic}^{(*1)}/C_{lic}^{(*1)}$, was the most significant feature for predicting conductivity within the given dataset.

The linear model with feature selection developed in this work offers a promising approach for material design support in advanced polymer development, where data availability is often limited. It provides both interpretability and reusability, which are critical for practical applications. Future work will focus on validating and generalizing this approach by incorporating a broader range of polymer structures and external datasets.

Acknowledgements

This work was supported by the MEXT Program: Data Creation and Utilization-Type Material Research and Development Project (Grant Number JPMXP1122715503). The authors also acknowledge the use of the RDE system provided through the DICE service (<https://dice.nims.go.jp/>) of the Materials Data Platform (MDPF), National Institute for Materials Science (NIMS), Japan. We thank Ms. Hiroko Nagao (NIMS) for the implementation of the tool used in this study, which is publicly available through the RDE system as template.

References

- [1] Park EJ, Jannasch P, Miyatake K, et al. Aryl ether-free polymer electrolytes for electrochemical and energy devices. *Chem Soc Rev.* 2024;53:5704–5780. Available from: <http://dx.doi.org/10.1039/D3CS00186E>.
- [2] Sriram G, Dhanabalan K, Ajeya KV, et al. Recent progress in anion exchange membranes (aems) in water electrolysis: synthesis, physio-chemical analysis, properties, and applica-

- tions. *J Mater Chem A*. 2023;11:20886–21008. Available from: <http://dx.doi.org/10.1039/D3TA04298G>.
- [3] Ahmed Mahmoud AM, Miyatake K. Optimization of the pendant chain length in partially fluorinated aromatic anion exchange membranes for alkaline fuel cells. *J Mater Chem A*. 2018;6:14400–14409. Available from: <http://dx.doi.org/10.1039/C8TA04310H>.
 - [4] Ahmed Mahmoud AM, Miyatake K. Highly conductive and alkaline stable partially fluorinated anion exchange membranes for alkaline fuel cells: Effect of ammonium head groups. *Journal of Membrane Science*. 2022;643:120072. Available from: <https://www.sciencedirect.com/science/article/pii/S0376738821010127>.
 - [5] Mohamed Ahmed Mahmoud A, Miyatake K. Highly conductive and ultra alkaline stable anion exchange membranes by superacid-promoted polycondensation for fuel cells. *ACS Applied Polymer Materials*. 2023;5(3):2243–2253. Available from: <https://doi.org/10.1021/acsapm.2c02227>.
 - [6] Mahmoud AMA, Miyatake K, Liu F, et al. Effect of radical-mediated cross-linking on partially fluorinated aromatic anion exchange membranes and their applications in alkaline water electrolysis cells. *Advanced Energy and Sustainability Research*. 2024; 5(3):2300236. Available from: <https://advanced.onlinelibrary.wiley.com/doi/abs/10.1002/aesr.202300236>.
 - [7] Nagata K, Kitazono J, Nakajima S, et al. An exhaustive search and stability of sparse estimation for feature selection problem. *IPJS Online Transactions*. 2015;8:25–32.
 - [8] Yasuhiko I, Hikaru T, Yoshinori NO, et al. Exhaustive search for sparse variable selection in linear regression. *Journal of the Physical Society of Japan*. 2018 04;87(4):044802. Available from: <https://cir.nii.ac.jp/crid/1524232505513522560>.
 - [9] Obinata K, Nakayama T, Ishikawa A, et al. Data integration for multiple alkali metals in predicting coordination energies based on bayesian inference. *Science and Technology of Advanced Materials: Methods*. 2022;2(1):355–364. Available from: <https://doi.org/10.1080/27660400.2022.2108353>.
 - [10] Geyer CJ. Markov chain monte carlo maximum likelihood. In: *Computing Science and Statistics: Proceedings of the 23rd Symposium on the Interface*; 1991. p. 156–163.
 - [11] Swendsen RH, Wang JS. Replica monte carlo simulation of spin-glasses. *Physical Review Letters*. 1986;57(21):2607–2609.
 - [12] Hukushima K, Nemoto K. Exchange monte carlo method and application to spin glass simulations. *Journal of the Physical Society of Japan*. 1996;65(6):1604–1608.
 - [13] Murakami R, Mizumaki M, Hamano Y, et al. Texture analysis of magnetic domain images using statistics based on human visual perception. *Journal of the Physical Society of Japan*. 2021;90(4):044705. Available from: <https://doi.org/10.7566/JPSJ.90.044705>.
 - [14] Simoncelli EP, the Laboratory for Computational Visio. *Pyrtools: tools for multi-scale image processing* ; 2025. Available from: <https://github.com/LabForComputationalVision/pyrtools/tree/v1.0.9>.
 - [15] Simoncelli EP, Freeman WT. The steerable pyramid: A flexible architecture for multi-scale derivative computation. In: *Proceedings of the 2nd IEEE International Conference on Image Processing*; Vol. 3; 1995. p. 444–447. Available from: <https://www.cns.nyu.edu/pub/eero/simoncelli95b.pdf>.

Table 1. Explanation of image features in this study.

Type	Name	Explanation
Brightness	P_μ	mean of brightness distribution
	P_σ	variance of brightness distribution
	P_k	kurtosis of brightness distribution
	P_s	skewness of brightness distribution
Frequency	HH	residual highpass feature
	LL	residual lowpass feature
	SP_{2048}	average magnitude of decomposition image (2048x2048)
	SP_{1024}	average magnitude of decomposition image (1024x1024)
	SP_{256}	average magnitude of decomposition image (256x256)
	SP_{128}	average magnitude of decomposition image (128x128)

8. Appendix

8.1. Explanation of image features

This section outlines the image features extracted from the TEM data used in this study. Specifically, we derived two types of features from the TEM images; brightness statistics P_μ , P_σ , P_k , P_s and frequency-domain features HH , LL , SP_{2048} , SP_{1024} , SP_{256} , SP_{128} obtained via wavelet transformation. A detailed description of each feature is provided in Table 1. In this study, the pixel size of the original TEM image input was 2048x2048. In Table 1, the SP_* is an abbreviation for the steerable pyramids, and the subscript indicates the size of the filtered image.

8.2. Correlation analysis between composition and TEM image

Section 6 suggested that frequency features derived from TEM images contain complementary information which correspond to the ratio of carbon numbers in hydrophilic and hydrophobic domains. To confirm this, we constructed a predictive model in which the TEM frequency features were used as explanatory variables, and the compositional feature $C_{bic}^{(*1)}/C_{lic}^{(*1)}$ was set as the response variable. Bayesian linear regression with automatic feature selection was employed. The results of feature selection are shown in Figure 7, where the y-axis represents the feature labels and the x-axis indicates the marginal posterior probability $P(g_m = 1 | \mathcal{D})$ for each feature.

As shown in Figure 7, three frequency features— HH , SP_{2048} , SP_{128} —were selected. The corresponding regression weights w_d for these features were $\{3.43, -2.68, 0.80\}$, respectively. Figure 8 presents the regression result based on the selected model estimated from the marginal probabilities.

From Figure 8, it can be seen that the compositional feature $C_{bic}^{(*1)}/C_{lic}^{(*1)}$ can be effectively approximated using only three frequency-domain features—i.e., features corresponding to specific spatial frequency bands in the TEM images. This indicates that the frequency-domain features do not provide complementary information with respect to conductivity prediction, but rather encode similar structural information already captured by the compositional descriptor.

Structurally, when the hydrophilic domain contains a higher number of carbon atoms, the side chains tend to be more flexible and spatially extended, facilitating the formation of larger and more interconnected hydrophilic domains. In contrast, a higher carbon content in the hydrophobic domain—particularly rigid structures such

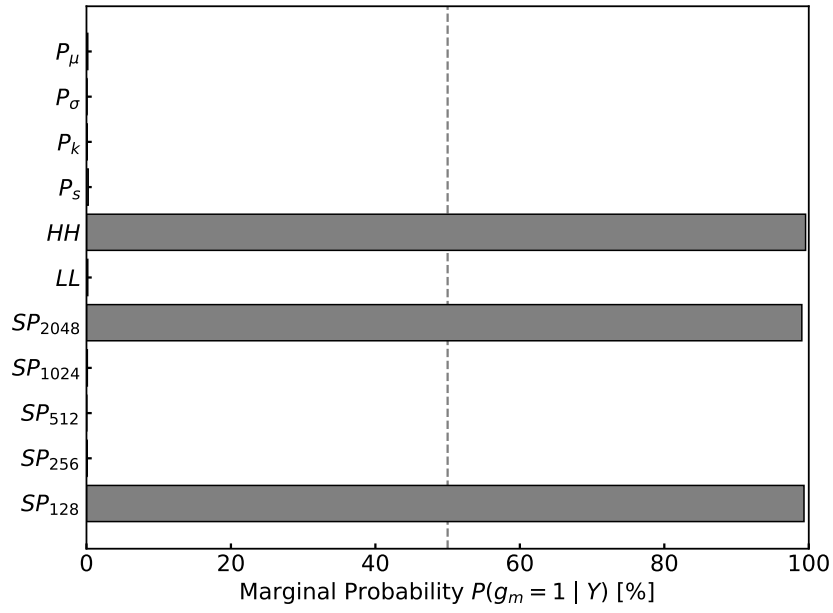


Figure 7. Result of feature selection based on the marginal log-likelihood. Candidate features was frequency features of TEM images. The wavy line indicates the prior probability of 50%. Object variable is $C_{bic}^{(*)}/C_{lic}^{(*)}$.

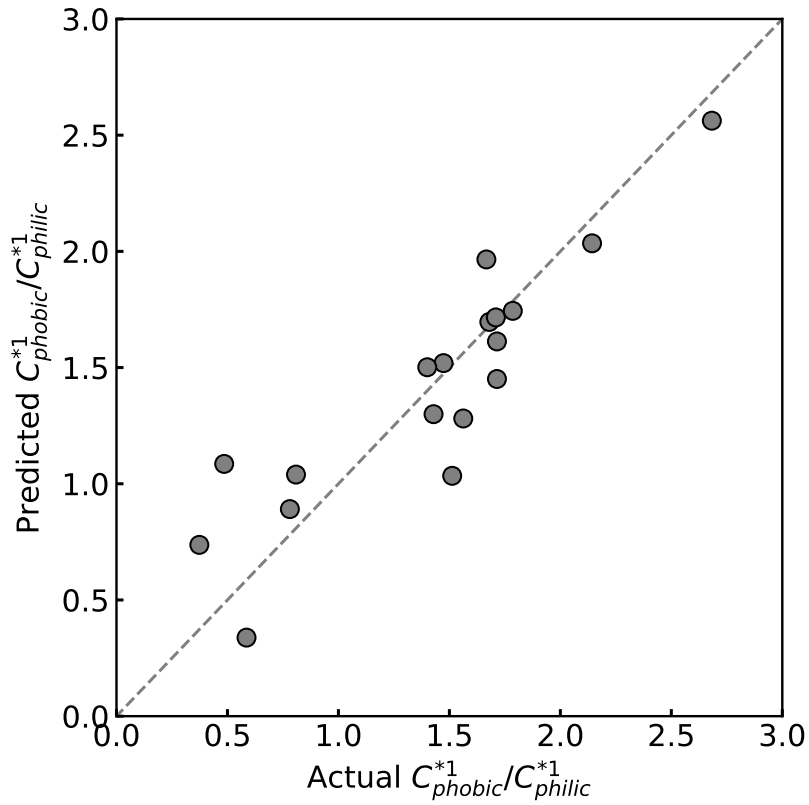


Figure 8. $C_{bic}^{(*)}/C_{lic}^{(*)}$ prediction result based on selected model

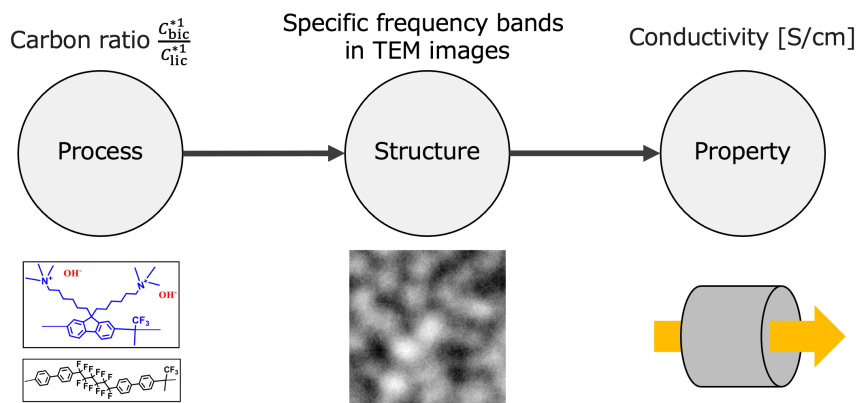


Figure 9. Relationships between processes, structures, and properties in this dataset organized based on model selection results.

as aromatic rings in the main chain—leads to an increased occupation of hydrophobic regions, which can fragment the hydrophilic domains. These structural differences are likely to manifest in the TEM images as variations in specific spatial frequency components, corresponding to domain size and connectivity.

Based on these computational experiments, the relationship among processing, structure, and properties can be summarized as shown in Figure 9. This process–structure–property correlation analysis suggests that the compositional ratio $C_{bic}^{(*1)}/C_{lie}^{(*1)}$ controls specific spatial frequency components in TEM images, thereby enhancing hydroxide ion conductivity.